Proc. Natl. Acad. Sci. USA
Vol. 92, pp. 9682–9686, October 1995
Neurobiology

Receptive field structure in the visual cortex: Does selective stimulation induce plasticity?

GREGORY C. DEANGELIS, AKIYUKI ANZAI, IZUMI OHZAWA, AND RALPH D. FREEMAN*

Group in Vision Science, School of Optometry, University of California, Berkeley, CA 94720-2020

Communicated by Russell L. De Valois, University of California, Berkeley, CA, July 12, 1995 (received for review February 28, 1995)

ABSTRACT **Sensory areas of adult cerebral cortex can reorganize in response to long-term alterations in patterns of afferent signals. This long-term plasticity is thought to play a crucial role in recovery from injury and in some forms of learning. However, the degree to which sensory representations in primary cortical areas depend on short-term (i.e., minute to minute) stimulus variations remains unclear. A traditional view is that each neuron in the mature cortex has a fixed receptive field structure. An alternative view, with fundamentally different implications for understanding cortical function, is that each cell's receptive field is highly malleable, changing according to the recent history of the sensory environment. Consistent with the latter view, it has been reported that selective stimulation of regions surrounding the receptive field induces a dramatic short-term increase in receptive field size for neurons in the visual cortex [Pettet, M. W. & Gilbert, C. D. (1992) *Proc. Natl. Acad. Sci. USA* 89, 8366–8370]. In contrast, we report here that there is no change in either the size or the internal structure of the receptive field following several minutes of surround stimulation. However, for some cells, overall responsiveness increases. These results suggest that dynamic alterations of receptive field structure do not underlie short-term plasticity in the mature primary visual cortex. However, some degree of short-term adaptability could be mediated by changes in responsiveness.**

Cortical maps exhibit substantial topographical reorganization following restricted deafferentation in adult mammals (1, 2). In the visual system, receptive fields (RFs) of neurons within a deafferented zone of primary visual cortex reorganize following retinal lesions (3–6). Recently, it has been reported that RF plasticity can be induced in normal adult cats by selective visual stimulation that mimics deafferentation. After several minutes of presentation of an artificial scotoma, in which regions surrounding a cell's RF are stimulated while the RF is masked, a 5-fold average expansion in RF area was observed (7, 8). This finding has fundamentally important implications, for it suggests that RFs in mature visual cortex are highly malleable over the course of seconds or minutes. In contrast, most prior studies of adult visual cortical neurons have tacitly assumed that response properties are fixed.

Using a sensitive, quantitative technique, we have sought to examine changes in the spatiotemporal structure of RFs resulting from an artificial scotoma and to characterize the mechanisms underlying this effect. Contrary to previous reports, however, we observe no change in either the size or internal structure of cortical RFs due to presentation of an artificial scotoma. Instead, for some cells, there is a reversible increase in response gain associated with surround stimulation. These gain changes appear to persist for no more than a few seconds once the RF is stimulated.

The publication costs of this article were defrayed in part by page charge payment. This article must therefore be hereby marked "*advertisement*" in accordance with 18 U.S.C. §1734 solely to indicate this fact.

MATERIALS AND METHODS

Preparation. Normal adult cats were prepared for single-unit recording experiments using standard surgical procedures that are described elsewhere (9). Our experimental preparation is similar in all respects to that used by Pettet and Gilbert (7). Responses of single neurons in striate cortex (area 17) were recorded extracellularly, while visual stimuli were presented on a high-resolution video display [mean luminance, 45 candelas (cd)/m^2]. For each isolated cell, preliminary tests were conducted with drifting sinusoidal gratings to determine the cell's preferred orientation and spatial frequency and to assess direction selectivity, binocularity, and surround inhibition. Cells were classified as simple or complex according to their RF organization (10) and also by the degree of temporal modulation in responses to gratings (11). Subsequently, all visual stimuli were presented to the eye that yielded the largest responses.

Experimental Protocol. Fig. 1*A* shows the protocol we used to study the effects of an artificial scotoma on RF structure. First, a reverse correlation technique (9, 12) was used to obtain a detailed map of the cell's RF (baseline measurement). Next, we filled the visual display with a conditioning stimulus and electronically masked out a region 1.5–3 times larger than the RF, thus creating an artificial scotoma. We have used four different types of conditioning stimuli, as shown in Fig. 1*B*. In each case, we confirmed that the conditioning stimulus alone did not excite the cell. After presenting the artificial scotoma for ≈10 min, blocks of the mapping stimuli were alternated with additional presentations of the conditioning stimulus. This alternation is needed because stimulation of the RF is reported to reverse the effects of the artificial scotoma (7). Finally, in the recovery test, we present a full-field conditioning stimulus for 5–10 min, followed by a normal sequence of mapping stimuli. This recovery test is necessary to assess whether changes in RF structure observed in the artificial scotoma condition are reversible.

RF Mapping. RF profiles were obtained by using a reverse-correlation technique (9, 12). Briefly, to obtain two-dimensional RF maps (e.g., Fig. 2), we present successive 25- to 50-ms flashes of a small bar stimulus at each of 20 × 20 locations on a stimulus grid (dashed square in Fig. 1*A*) that contains the entire RF and is rotated to match the cell's preferred orientation. Two-dimensional response histograms are accumulated (for a given correlation delay, T) by assigning each spike to the location of the stimulus that preceded it by T ms. For simple cells, a composite RF profile is obtained by taking the difference of separate bright- and dark-bar response histograms. This analysis is repeated for a range of correlation delays to yield a complete spatiotemporal RF profile (9, 13). In this report, we present spatial RF profiles obtained at the optimal correlation delay (the delay that yields the profile having maximal signal-to-noise ratio).

Abbreviations: RF, receptive field; AS/B, artificial scotoma/baseline ratio; R/AS, recovery, artificial scotoma ratio.

*To whom reprint requests should be addressed.

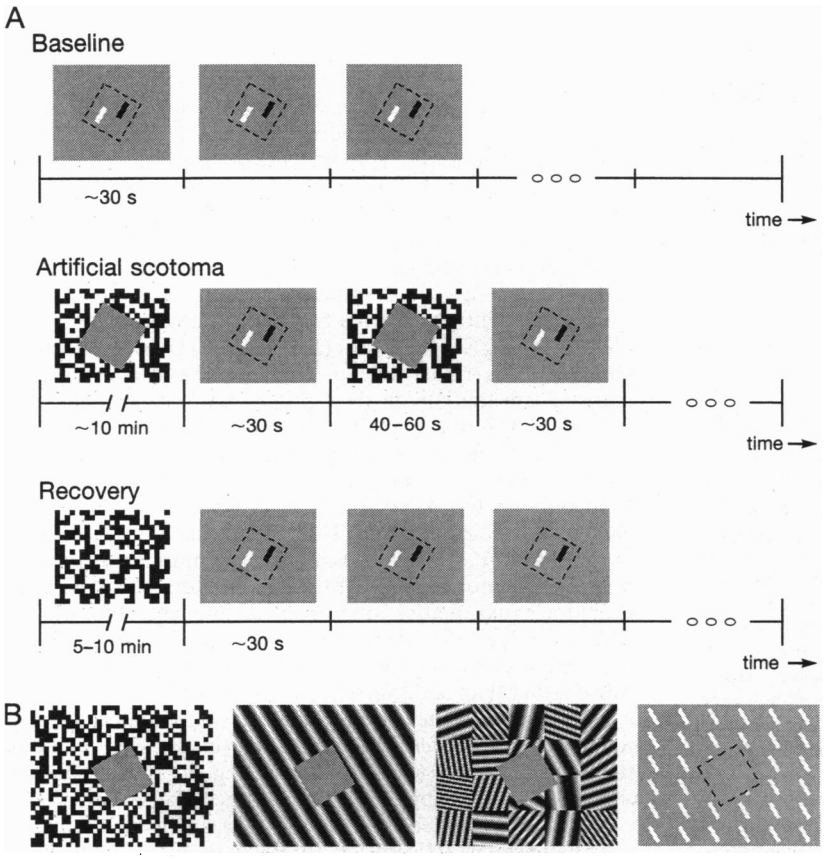

FIG. 1. (*A*) A three-stage experimental protocol is used to assess the effect of an artificial scotoma on RF structure. In the "Baseline" test, a pseudorandom sequence of small flashed bar stimuli is used to map the RF quantitatively. This stimulus sequence is partitioned into a series of blocks, each of which lasts ≈30 s. During one block, each position on the 20 × 20 stimulus grid (dashed square) is tested once with a bright bar and once with a dark bar. The sequence is randomized for each successive block, and 20–50 blocks are typically presented. In the "Artificial scotoma" test, a region of the display somewhat larger than the stimulus grid is blank (mean luminance), while the surrounding regions are stimulated with one of four visual patterns shown in *B*. After ≈10 min of presentation of this artificial scotoma, blocks of the mapping stimulus are alternated with additional periods (typically 40–60 s) of the artificial scotoma. In the "Recovery" test, the artificial scotoma is removed, and the full field is stimulated for a period of 5–10 min; this is followed by a normal series of blocks of the mapping stimulus. Note that the mapping stimuli are identical in the baseline, scotoma, and recovery conditions. (*B*) The four different types of conditioning stimuli used in these experiments are shown from left to right: a pattern of dynamic random dots, a single grating drifting at the cell's optimal orientation, a grating patchwork in which each patch has a randomly chosen orientation and spatial frequency, and a pattern of optimally oriented (or, in a few cases, randomly oriented) moving bars. In each case, the display subtends 28° × 22°, and the artificial scotoma is created by electronically masking out a rectangular portion of the pattern (shown as a dashed square for the moving bar pattern).

In our initial experiments, we examined the effects of an artificial scotoma on two-dimensional RF profiles, obtained as described above. In later experiments, to reduce the length of the mapping periods that are interspersed with conditioning periods (see Fig. 1*A*), we also used a one-dimensional version of the mapping stimulus (9). In the one-dimensional version, bar length was set equal to the length of the stimulus grid (i.e., somewhat longer than the RF), and bar width was typically 0.2–0.5°. By presenting optimally oriented bars at 20 equally spaced positions along the axis of the RF perpendicular to the preferred orientation, we obtain a one-dimensional map of RF sensitivity (e.g., Fig. 3).

Quantitative Analysis. To obtain a quantitative summary of results (see Fig. 4), we analyzed one-dimensional RF profiles that were obtained before, during, and after conditioning with an artificial scotoma. Each one-dimensional RF profile was fit with an appropriate curve (see Fig. 3) by minimizing the sum-squared error between data and fit as described in more detail elsewhere (9, 14). For complex cells, as well as a subpopulation of simple cells (7/37) that had spatially unimodal RFs, profiles obtained from responses to either bright or dark bars (whichever was larger) were fit with a Gaussian function having the form:

$$R(x) = R_0 + K \exp(-(x - x_0)^2/a^2).$$

In this formulation, R_0 is the base response rate, K is the amplitude, x_0 is the center position, and a is the size (half-width at e^{-1} of the dynamic range) of the RF. For multimodal simple cells, RF profiles (computed as the difference of bright- and dark-bar responses) were fit with a Gabor function:

$$R(x) = K \exp(-(x - x_0)^2/a^2)\cos(2\pi f_{opt}(x - x_0) + P).$$

This function is simply a Gaussian envelope (having the same parameters described above) multiplied by a sinusoid that has spatial frequency, f_{opt}, and phase, P. Note that, for multimodal simple cells, the base rate, R_0, was derived directly from the response histograms for bright and dark bars (average response level outside the RF envelope); otherwise, the base rate would be eliminated upon subtracting the dark-bar response from the bright-bar response.

The Gaussian and Gabor functions used here have been shown previously to provide good fits to the RFs of complex cells (15) and simple cells (16, 19), respectively. Although other formulas may fit the data equally well, we have chosen these functions mainly because they have easily interpretable parameters, such as size, spatial frequency, and phase.

RESULTS

We have recorded extracellularly from 102 neurons in area 17 of 11 anesthetized and paralyzed adult cats; from this population, 79 cells were studied in detail. Two-dimensional RF profiles obtained before, during, and after conditioning with an artificial scotoma are shown in Fig. 2. For the complex cell of Fig. 2*A*, there is no obvious change in RF size, shape, or amplitude (i.e., responsiveness) due to an artificial scotoma. For the simple cell of Fig. 2*B*, there is a small sequential decline (from left to right) in response amplitude, but no change in RF size or shape. Note that the gradual decline in amplitude for this simple cell cannot be attributed to the artificial scotoma because the effect was not reversible. We have obtained similar data for 24 cells, 14 simple and 10 complex. Changes in RF structure were quantified for each cell by fitting appropriate two-dimensional functions to the data (19) and comparing parameters obtained from the baseline, artificial scotoma, and recovery conditions. In short, there was no significant tendency for any parameter of the RF to change in a reversible manner because of the artificial scotoma. In particular, we find no change in RF size or shape, as illustrated by the examples of Fig. 2.

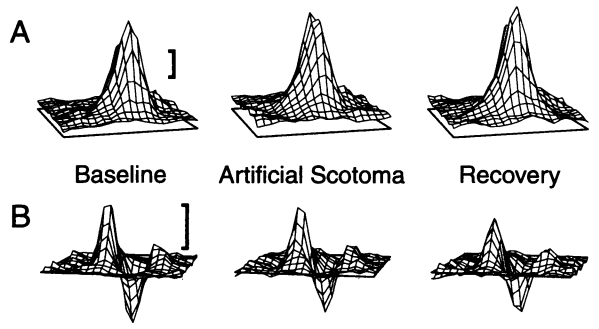

FIG. 2. (*A*) RF profiles for a complex cell obtained before (*Left*), during (*Center*), and after (*Right*) conditioning with an artificial scotoma. In these surface plots, response to bright bars is plotted as a function of two dimensions of visual space; the reverse correlation delay is 60 ms. Response profiles obtained with dark bars were nearly identical (17, 18). Note that all three profiles are plotted on the same absolute response scale, in terms of spikes per stimulus (i.e., the average number of spikes elicited by a single flash of a bar stimulus at each position). The scale bar shows an increment of 1 spike per stimulus. For this cell, the mapping stimuli were 1° × 0.35° bars, the stimulus grid subtended 7° × 7°, and the artificial scotoma measured 9.5° × 10°. The conditioning stimulus was a pattern of dynamic random dots. (*B*) RF profiles for a simple cell plotted in the same format as those in *A*. For simple cells, we plot the difference between responses to bright and dark bars (9, 12) so that positive and negative peaks represent bright- and dark-excitatory subregions, respectively. The reverse-correlation delay is 55 ms. The mapping stimuli were 1.5° × 0.5° bars, the stimulus grid was 8° × 8°, the artificial scotoma subtended 9° × 9°, and the conditioning stimulus was a pattern of dynamic random dots.

One possible reason that we did not observe RF expansion is that the field collapses back to its original size when stimulated (7). If this occurs very rapidly (within a few seconds), then our mapping periods (see Fig. 1*A*) may have been too long (≈30 s) to observe the effect. To test this possibility, we used a one-dimensional variant of the mapping algorithm (see *Materials and Methods*), thus reducing the duration of our mapping periods to 1–2 s. The duration of interleaved conditioning stimuli in the artificial scotoma test was also reduced to 20–30 s; otherwise, all aspects of the modified protocol were as shown in Fig. 1*A*.

With this modified protocol, we still failed to observe any clear, reversible changes in RF size or shape, but we did see reversible changes in responsiveness for some cells. Fig. 3 shows representative results for three neurons. For the complex cell of Fig. 3*A*, raw data (Fig. 3*A Left*) show that both the base response rate (plateau level) and response amplitude increase substantially in the artificial scotoma condition and subsequently return to their original values in the recovery test. However, when these one-dimensional profiles are simply scaled to have the same peak response (Fig. 3*A Middle*), they fall nearly on top of one another, indicating that there is no change in RF size or shape. These relationships are quantified in Fig. 3*A Right*, which shows the relative amplitudes (normalized to baseline values) of fitted parameters obtained under the three experimental conditions (see the legend for details). This matching of scaled RF profiles suggests that the increase in response gain associated with an artificial scotoma is multiplicative rather than additive. The simple cell of Fig. 3*B* also shows a large reversible increase in response amplitude due to the scotoma (Fig. 3*B Left*), but no change in the size or internal structure of the RF (Fig. 3*B Middle*). Fig. 3*C* shows data for a simple cell that exhibited no clear changes whatsoever.

We have examined the effects of an artificial scotoma on one-dimensional RF profiles for 55 neurons: 37 simple cells

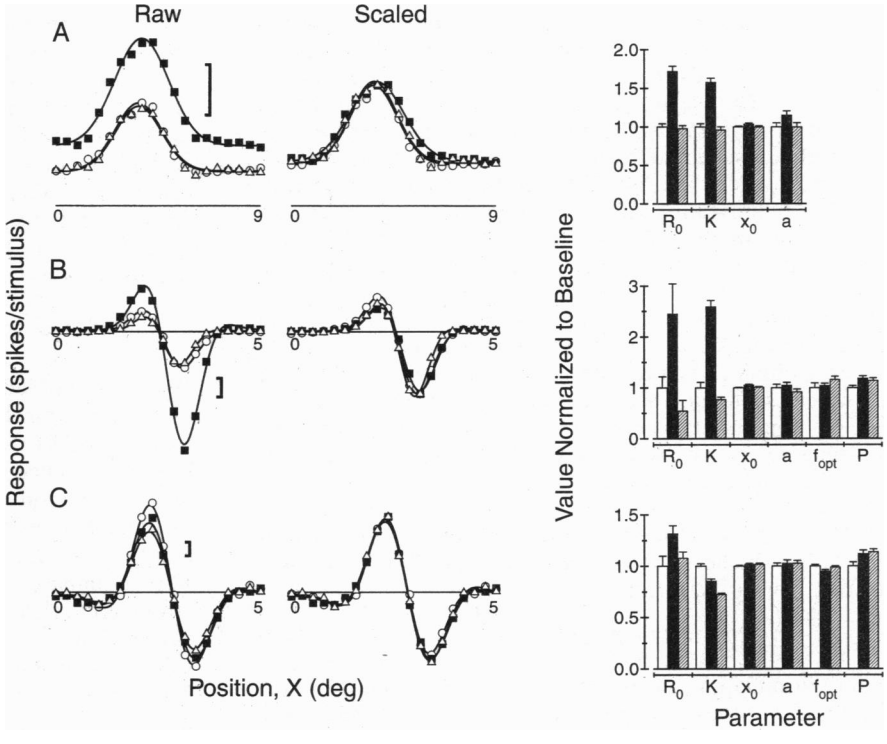

FIG. 3. Effects of an artificial scotoma on one-dimensional RF profiles for three neurons. Open circles, filled squares, and open triangles represent data obtained in the baseline, artificial scotoma, and recovery conditions, respectively. (*Left*) For each cell, raw RF profiles are shown plotted on an absolute response scale in spikes per stimulus (scale bars show an increment of 1 spike/stimulus). (*Middle*) Scaled profiles are shown. To scale the data, each profile is simply multiplied by an appropriate factor so that the maximum absolute values of the data are equal. (*Right*) Summary of changes in RF parameters are shown. White, black and gray bars show the relative values of each parameter of the fit for the baseline, artificial scotoma, and recovery conditions, respectively. For each parameter (see *Materials and Methods* for definitions), all three values are normalized to the value obtained in the baseline condition (i.e., all white bars have a value of 1.0). Error bars represent one standard error of the estimate values. (*A*) One-dimensional RF profiles are shown for a complex cell. Solid curves show the Gaussian function that best fits each profile. The raw data (*A Left*) show a clear, reversible increase in both the base response rate (R_0) and the amplitude (K) of the RF profile. However, the scaled data (*A Middle*) show that there is very little change in either the size or shape of the RF. For this cell, the mapping stimuli were 9° × 0.35° bars, the stimulus grid was 9° across, and the reverse-correlation delay was 67 ms. The conditioning stimulus was a pattern of dynamic random dots, and the artificial scotoma measured 9.5° × 11°. (*B*) Data are shown for a simple cell that exhibits a large, reversible increase in response amplitude (K) due to the artificial scotoma. Again, there is little change in RF size or shape when the response profiles are scaled (*B Middle*). Solid curves show the best-fitting Gabor functions. Mapping stimuli were 5° × 0.3° bars, grid size was 5°; reverse-correlation delay was 78 ms; and scotoma size was 5° × 8°. (*C*) Data from a simple cell for which the artificial scotoma had no clear effect. The raw profiles (*C Left*) show a small, gradual decrease in response amplitude from the baseline to the scotoma condition and again from the scotoma to the recovery condition. RF profiles match almost exactly when scaled (*C Middle*). Mapping stimuli were 5° × 0.4° bars; grid size was 5°; reverse-correlation delay was 80 ms; and scotoma size was 5.5° × 5°.

and 18 complex cells. Results were quantified by fitting an appropriate function (solid curves in Fig. 3) to each one-dimensional profile and extracting parameter values (see *Materials and Methods*). A parametric summary of the data is given in Fig. 4. For response amplitude (K), a majority of data points cluster in the lower right quadrant of the scatter plot (Fig. 4*A*), indicating that there is a reversible increase in K due to the artificial scotoma. The median value of the artificial scotoma/baseline (AS/B) ratio for K is 1.20, which is significantly greater than 1 (Wilcoxon signed-rank test, $P < 0.001$). Similarly, the median value of the recovery/artificial scotoma (R/AS) ratio for K is 0.74, which is significantly smaller than 1 ($P < 0.001$). Note, however, that some cells do not exhibit any change in response amplitude. A very similar pattern of results can be seen in Fig. 4*B* for the base rate parameter, R_0 (median of AS/B = 1.38, $P < 0.001$; median of R/AS = 0.71, $P < 0.001$).

Whereas amplitude and base rate show a clear trend to increase during the artificial scotoma (and then recover), the remaining RF parameters do not. Data points in Fig. 4 *C–F* cluster around the center of each scatter diagram. For RF size, a (Fig. 4*C*), the median AS/B ratio (1.03) is marginally larger than 1 ($P = 0.015$), but the median R/AS ratio (0.98) is not significantly smaller than 1 ($P = 0.12$). Clearly, changes in size are minimal compared with changes in amplitude or base rate. Moreover, there is a significant correlation ($r = 0.40$, $P = 0.0005$) between changes in RF size and changes in base rate, which suggests that the small size changes shown by some cells may result from a weak "iceberg effect" associated with the much larger changes in base rate. Fig. 4*D* shows that there is no significant change in the optimal spatial frequency, f_{opt}, of simple cells due to an artificial scotoma (median of AS/B = 0.98, $P = 0.21$; median of R/AS = 1.003, $P = 0.26$). Similarly, Fig. 4*E* shows that there are no consistent changes in RF center position, x_0 (median of AS − B = −0.03°, $P = 0.45$; median of R − AS = 0.03°, $P = 0.78$). Some of the scatter in Fig. 4*E* is probably due to small shifts in eye position that occurred during the three-stage testing sequence. However, relative to the size of the RF, the largest positional shift that occurred was only 15%, and, in most cases (53 of 77), the shifts were <5% of the full width of the RF. Lastly, Fig. 4*F* shows that there is no consistent change in the spatial phase, P, of simple cell RFs (median of AS − B = 0.01°, $P = 0.47$; median of R − AS = 0.02°, $P = 0.24$).

There were no significant differences between simple and complex cells with regard to any of the parameter ratios or differences shown in Fig. 4 (ANOVA, $P > 0.05$). For amplitude (K) and base rate (R_0), AS/B ratios tended to be larger (and R/AS ratios tended to be smaller) for the random dot and patchwork conditioning stimuli than for the single grating and moving bar patterns, but these differences were also not significant (ANOVA, $P > 0.05$).

Fig. 4 demonstrates that there is no scotoma-induced change in the size or structure of the RF along the axis perpendicular to the cells' preferred orientation. For 10 cells (6 simple, 4 complex), we have also analyzed one-dimensional profiles obtained along the length axis of the receptive field (parallel to the preferred orientation). These data show a pattern of results similar to that in Fig. 4. We also have analyzed temporal RF profiles (9) for the same population of cells represented in Fig. 4, and we find a nearly identical pattern of results. Thus, we conclude that an artificial scotoma can increase the gain of a cell's response but has no effect on the spatiotemporal structure of its RF. The increase in response gain (e.g., Fig. 3 *A* and *B*) could result directly from prolonged stimulation of the surround or could result from habituation of the response to mapping stimuli in the baseline and recovery conditions. In the latter case, the increased gain we have observed would simply result from a lack of cell activation during the artificial scotoma periods. To control for this possibility, we inserted 15- to 20-s blank periods (i.e., no visual stimulus) between blocks of mapping stimuli in the baseline and recovery trials, and we retested 10 cells that showed a clear gain increase without blanks. For four cells, the gain increase was maintained when blank periods were inserted; however, for six cells, the gain change was eliminated or drastically reduced. This suggests that some, but not all, of the effects seen in Fig. 4 *A* and *B* resulted from adaptation to the mapping stimuli rather than from stimulation of the surround.

DISCUSSION

This study addresses a fundamental question regarding cortical processing: is the representation of a visual scene in adult

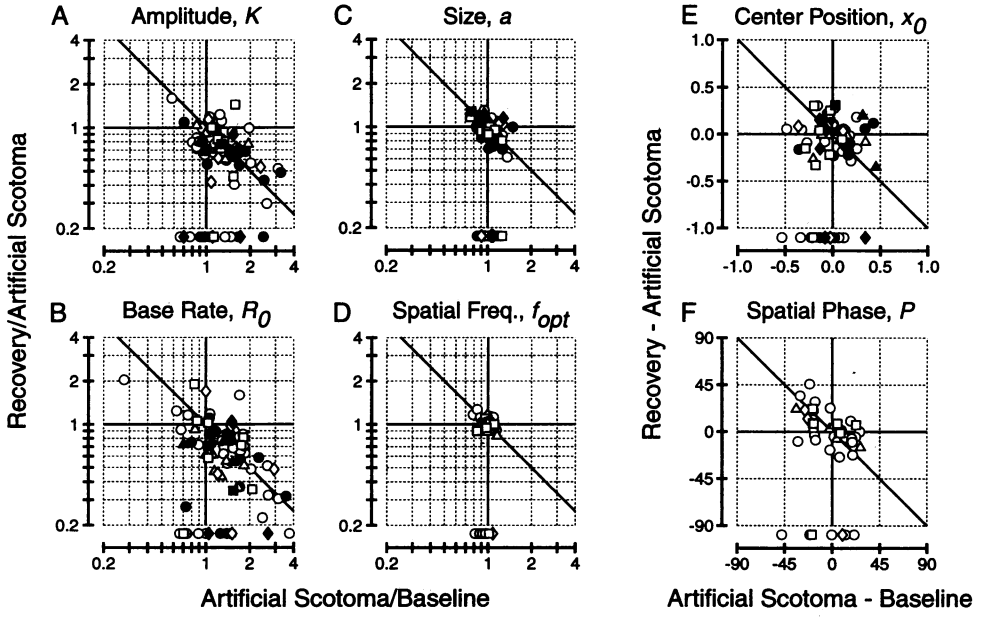

FIG. 4. Quantitative summary of changes in RF structure due to an artificial scotoma. Data are shown for 77 test sequences performed on 55 cells (some cells were tested with two or more different conditioning stimuli). Open and filled symbols represent simple and complex cells, respectively. The different symbol types in each scatter plot denote test sequences performed using the four types of conditioning stimuli shown in Fig. 1*B*: dynamic random dots (circles, $n = 47$), a single drifting grating (triangles, $n = 11$), a grating patchwork (diamonds, $n = 9$), and a pattern of optimally ($n = 7$) or randomly ($n = 3$) oriented moving bars (squares). Each panel summarizes changes in one RF parameter: amplitude (K) (*A*), base rate (R_0) (*B*), size (a) (*C*), optimal spatial frequency (f_{opt}) (*D*), center position (x_0) (*E*), and spatial phase (P) (*F*). For parameters that are non-zero and positive (*A–D*), we plot parameter ratios. On the horizontal axis, we plot the parameter value obtained in the artificial scotoma condition divided by the parameter value obtained in the baseline test (AS/B ratio); on the vertical axis, we plot the recovery value divided by the artificial scotoma value (R/AS ratio). For parameters that can be positive or negative (*E* and *F*), we plot differences (i.e., AS − B and R − AS) between parameter values instead of ratios. Data points plotted just above the horizontal axis in each panel denote test sequences for which the cell was lost before a recovery run could be completed.

primary visual cortex (V1) fixed or does it change from minute to minute depending on sensory context? A traditional ("bottom-up") view, rooted in the notion of feed-forward hierarchical processing, is that the stimulus–response characteristics of V1 cells are fixed and that more elaborate representations of the world are constructed in successively higher cortical areas from the output of V1 (10, 20). Alternatively, the stimulus–response properties of V1 neurons may be dynamically adjusted, perhaps by virtue of horizontal connections or feedback from higher cortical areas ("top-down" processing), to tailor the V1 representation for further processing (21, 22). If the latter view is correct, then it should be possible to observe changes in RF structure that depend on stimulus context.

Gilbert and colleagues (7, 8) have recently reported that selective stimulation of regions surrounding the classical RF induces a several-fold increase in RF area. They suggest that synaptic connections are modified so that surround stimulation unmasks excitatory influences from regions outside the classical RF (21). In contrast, we have found no change in the size or detailed structure of cortical RFs due to surround stimulation, but we have observed dynamic changes in response gain. It seems quite unlikely that we missed the 5-fold changes in RF area reported previously because our animal preparation and experimental protocol are very similar to those used by Gilbert and colleagues (7, 8). In addition, our RF mapping and analysis procedures are quite sensitive to small changes in RF parameters, as illustrated by the magnitudes of the error bars in Fig. 3 *Right*. For example, the average standard error of our size estimates, expressed as a percentage of the fitted value, was 6.6 $\pm$ 0.4%. Thus, if RF size had increased by a factor of 2 or more, as reported (7, 8), our analysis could certainly have detected the change. Also, the overall quality of fits was not significantly different (ANOVA, $P = 0.58$) among the three experimental conditions (average rms errors were as follows: baseline, 11.89 $\pm$ 0.68%; artificial scotoma, 12.02 $\pm$ 0.67%; recovery, 12.89 $\pm$ 0.79%), which discounts the possibility that scotoma-induced changes in RF structure were not captured by the Gaussian and Gabor models used to fit the data. We suggest that the major difference between our results and those reported previously involves the definition of RF size. If one measures size using an absolute-response-level criterion, then changes in response amplitude or base rate could be interpreted as changes in RF size. This may have been the case in the previous studies because they relied principally on hand-plotting of RFs. We contend, however, that RF size should be defined independently of response amplitude, as is commonly done for measurements of orientation or spatial frequency bandwidth (23, 24). By this definition, we find no change in RF size due to an artificial scotoma. Indeed, some of the quantitative data presented by Pettet and Gilbert (7) also appear to be more consistent with a gain increase than with a size increase [e.g., their figure 4 (7)].

Our results rebut the idea (21) that synaptic inputs from regions surrounding the classical RF are selectively enhanced by an artificial scotoma. Instead, our findings suggest that some influence uniformly elevates the gain of all inputs to a cell rather than selectively enhancing those from the surround. These two scenarios (size change vs. gain change) have fundamentally different implications for visual information processing. A large change in RF size would be accompanied by changes in the basic filtering properties of a neuron, such as its spatial frequency selectivity. In contrast, our findings demonstrate that the basic spatiotemporal tuning properties of striate cortex neurons are unaffected by selective stimulation—only responsiveness changes. We speculate that the observed increase in response gain may result from adaptation of inhibitory inputs from regions outside the classical RF. These inputs may be mediated by long-range horizontal connections in the cortex (25, 26). If each cell receives divisive (i.e., shunting) inhibition (27) from a pool of cells with spatially displaced RFs and if the response of this pool of cells adapts to prolonged stimulation (thus reducing inhibition), this would cause a multiplicative increase in response magnitude for the neuron under study (28). Note that these changes in response gain must be relatively short-lived because we only observe them when our RF mapping periods are very brief (1–2 s).

Our findings suggest that the RF structure of V1 cells does not depend on the recent history of visual stimulation. This argues against a highly dynamic representation of the visual scene in V1. However, our results do leave open the possibility that dynamic changes in response gain may endow some V1 neurons with a limited degree of short-term adaptability. The gain changes described here could account for some reported psychophysical phenomena (29–31), such as perceptual filling-in.

We thank M. W. Pettet for helpful conversations during the course of this study. This work was supported by National Eye Institute Grant EY01175 and by the Human Frontiers Science Program.

1. Kaas, J. H. (1991) *Annu. Rev. Neurosci.* **14,** 137–167.
2. Garraghty, P. E. & Kaas, J. H. (1992) *Curr. Opin. Neurobiol.* **2,** 522–527.
3. Kaas, J. H., Krubitzer, L. A., Chino, Y. M., Langston, A. L., Polley, E. H. & Blair, N. (1990) *Science* **248,** 229–231.
4. Heinen, S. J. & Skavenski, A. A. (1991) *Exp. Brain Res.* **83,** 670–674.
5. Chino, Y. M., Kaas, J. H., Smith, E. L., III, Langston, A. L. & Cheng, H. (1992) *Vision Res.* **32,** 789–796.
6. Gilbert, C. D. & Wiesel, T. N. (1992) *Nature (London)* **356,** 150–152.
7. Pettet, M. W. & Gilbert, C. D. (1992) *Proc. Natl. Acad. Sci. USA* **89,** 8366–8370.
8. Volchan, E. & Gilbert, C. D. (1995) *Vision Res.* **35,** 1–6.
9. DeAngelis, G. C., Ohzawa, I. & Freeman, R. D. (1993) *J. Neurophysiol.* **69,** 1091–1117.
10. Hubel, D. H. & Wiesel, T. N. (1962) *J. Physiol. (London)* **160,** 106–154.
11. Skottun, B. C., De Valois, R. L., Grosof, D. H., Movshon, J. A., Albrecht, D. G. & Bonds, A. B. (1991) *Vision Res.* **31,** 1079–1086.
12. Jones, J. P. & Palmer, L. A. (1987) *J. Neurophysiol.* **58,** 1187–1211.
13. McLean, J., Raab, S. & Palmer, L. A. (1994) *Visual Neurosci.* **11,** 271–294.
14. DeAngelis, G. C., Ohzawa, I. & Freeman, R. D. (1995) *Perception* **24,** 3–31.
15. Baker, C. L., Jr., & Cynader, M. S. (1986) *J. Neurophysiol* **55,** 1136–1152.
16. Marcelja, S. (1980) *J. Opt. Soc. Am.* **70,** 1297–1300.
17. Movshon, J. A., Thompson, I. D. & Tolhurst, D. J. (1978) *J. Physiol. (London)* **283,** 79–99.
18. Ohzawa, I., DeAngelis, G. C. & Freeman, R. D. (1990) *Science* **249,** 1037–1041.
19. Jones, J. P. & Palmer, L. A. (1987) *J. Neurophysiol.* **58,** 1233–1258.
20. Barlow, H. B. (1972) *Perception* **1,** 371–394.
21. Gilbert, C. D. (1992) *Neuron* **9,** 1–13.
22. Olshausen, B. A., Anderson, C. H. & Van Essen, D. C. (1993) *J. Neurosci.* **13,** 4700–4719.
23. Campbell, F. W., Cleland, B. G., Cooper, G. F. & Enroth-Cugell, C. (1968) *J. Physiol. (London)* **198,** 237–250.
24. Movshon, J. A., Thompson, I. D. & Tolhurst, D. J. (1978) *J. Physiol. (London)* **283,** 101–120.
25. Gilbert, C. D. & Wiesel, T. N. (1983) *J. Neurosci.* **3,** 1116–1133.
26. McGuire, B. A., Gilbert, C. D., Rivlin, P. K. & Wiesel, T. N. (1991) *J. Comp. Neurol.* **305,** 370–392.
27. Heeger, D. J. (1992) *Visual Neurosci.* **9,** 181–197.
28. Xing, J. & Gerstein, G. L. (1994) *Vision Res.* **34,** 1901–1911.
29. Ramachandran, V. S. & Gregory, R. L. (1991) *Nature (London)* **350,** 699–702.
30. Kapadia, M. K., Gilbert, C. D. & Westheimer, G. (1994) *J. Neurosci.* **14,** 451–457.
31. Hardage, L. & Tyler, C. W. (1995) *Vision Res.* **35,** 757–766.